JACS
JOURNAL OF THE AMERICAN CHEMICAL SOCIETY

Article

pubs.acs.org/JACS

Single-Molecule Nanocatalysis Reveals Catalytic Activation Energy of Single Nanocatalysts

Tao Chen,[†,‡] Yuwei Zhang,[†] and Weilin Xu*[,†]

[†]State Key Laboratory of Electroanalytical Chemistry and Jilin Province Key Laboratory of Low Carbon Chemical Power, Changchun Institute of Applied Chemistry, Chinese Academy of Science, 5625 Renmin Street, Changchun 130022, P. R. China

[‡]Graduate University of Chinese Academy of Science, Beijing 100049, P. R. China

Supporting Information

ABSTRACT: By monitoring the temperature-dependent catalytic activity of single Au nanocatalysts for a fluorogenic reaction, we derive the activation energies via multiple methods for two sequential catalytic steps (product formation and dissociation) on single nanocatalysts. The wide distributions of activation energies across multiple individual nanocatalysts indicate a huge static heterogeneity among the individual nanocatalysts. The compensation effect and isokinetic relationship of catalytic reactions are observed at the single particle level. This study exemplifies another function of single-molecule nanocatalysis and improves our understanding of heterogeneous catalysis.

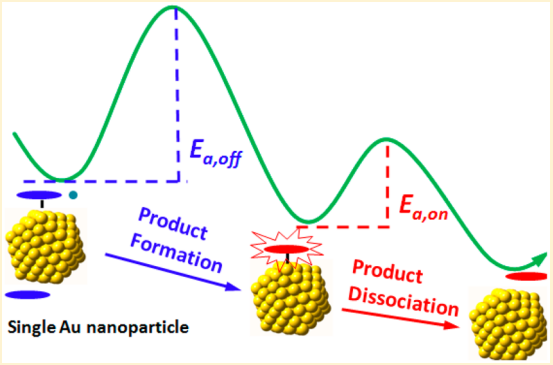

INTRODUCTION

Nanocatalysts have been actively studied in recent decades due to their extensive applications in many fields.[1] Investigation of the catalytic characteristics of nanomaterials is particularly significant, since such investigations can potentially guide the rational design of highly effective catalysts. Recently, on the basis of fluorescence-based single-molecule investigation of nanocatalysis, some new catalytic properties (such as the heterogeneous reaction pathways and catalytic dynamics, the distribution of active sites, size- or facet-dependent catalysis, etc.) of single nanocatalysts have been successfully revealed at the single-molecule level.[2−13]

Catalytic activation energy (E_a) measures the chemical activity of a catalyst and controls the rate-limiting step of the whole catalysis process,[1] thus making it one of the most important kinetic parameters. However, traditional ensemble experiments on nanomaterials can only measure an average activation energy of the rate-limiting step of the entire catalytic cycle (including multiple steps).[14,15] The compensation effect, a linear correlation between activation energy (E_a, which determines the temperature dependence) and frequency factor (A, which determines the over rate) in the Arrhenius dependence, which is often called the compensation (or Constable−Cremer) law,[16,17] has been predicted and observed extensively for many thermally activated processes since its discovery in 1908.[18−25] The compensation effect is related to, but distinct from, the so-called isokinetic relationship.[23,24] It has been known that the compensation effect could be useful in chemical research for identifying the governing reaction mechanism, predicting Arrhenius parameters when limited data are available, predicting effects of various parameters on reactions, separating the effects of surface and bulk properties, and optimizing process design.[26] However, conventional ensemble observation of compensation law on nanocatalysts is only for an entire catalytic cycle without discriminating different steps, since the ensemble method only can obtain an averaged activation energy of the rate-limiting step of the entire catalytic cycle (including multiple steps).[14,15]

In this work, on the basis of a fluorogenic reaction catalyzed by individual Au nanocatalysts, by adding the powerful new independent variable of temperature to the single-molecule nanocatalysis and differentiating the two steps of a tandem reaction sequence—product formation followed by product dissociation—on a single-molecule nanocatalysis, for the first time, we obtained the activation energies ($E_{a,i}$, i = off or on) for both product formation and dissociation processes of a fluorogenic reaction catalyzed by single nanocatalysts. We observed that a smaller activation energy usually corresponds to higher intrinsic catalytic activity on a single nanocatalyst. More importantly, a compensation effect between $E_{a,i}$ and the frequency factor (A) from the Arrhenius equation and isokinetic relationship were also observed at the single particle level. This study exemplifies another function of single-molecule nanocatalysis.

RESULTS AND DISCUSSION

Rates of a Fluorogenic Reaction Catalyzed by a Single Nanocatalyst at Different Temperatures. In this work, a

Received: June 1, 2016
Published: August 31, 2016

DOI: 10.1021/jacs.6b05600
J. Am. Chem. Soc. 2016, 138, 12414−12421

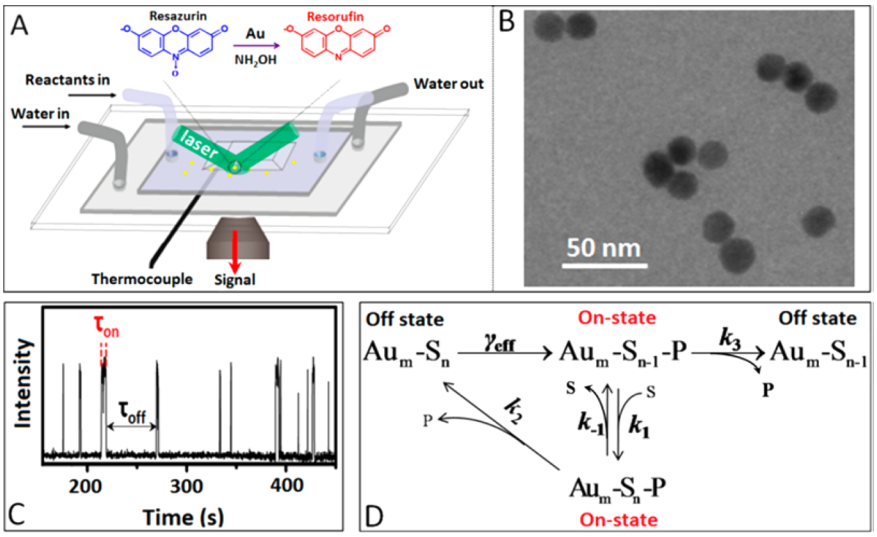

Figure 1. (A) Scheme of temperature-controllable single-molecule nanocatalysis based on a fluorogenic reaction with Resorufin as the product. (B) Typical TEM image of 18.3 nm Au nanoparticles. (C) Exemplary fluorescence intensity versus time trajectory of a single Au nanoparticle with 50 nM Resazurin and 5 μM NH_2OH at 25 °C. Time resolution: 100 ms. (D) Langmuir−Hinshelwood mechanism of single-molecule nanocatalysis: Au_m, Au nanoparticles; S, the substrate Resazurin; P, the product Resorufin; [S], substrate concentration; Au_m−S_n represents one Au nanoparticle having n adsorbed substrate molecules; γ_{eff}, the effective rate constant representing the combined reactivity of all surface sites on one Au nanoparticle; k_1, k_{-1}, k_2, k_3, the rate constants for substrate adsorption and product dissociation.

classic fluorogenic reduction reaction between nonfluorescent Resazurin and hydroxylamine catalyzed by Au nanocatalysts (Supporting Information, Figure S1) was adopted to study the reaction kinetics of individual nanoparticles at different temperatures. As shown in Figure 1A, the fluorescent product molecules Resorufin formed on the surface of a Au nanoparticle were sequentially detected using a wide-field single-molecule fluorescence microscope. In order to study the catalytic process on the same single nanoparticle at different temperatures, a homemade, temperature-controllable (error ±0.2 °C at temperature controller in the range 20−45 °C, Supporting Information) flow cell was fabricated as shown in Figure 1A with a recycling water bath (Figure S2). First, we studied the single-molecule nanocatalysis of individual 18.3 nm Au nanoparticles (Figure 1B and Figure S3) at 25 °C. Figure 1C shows part of an exemplary fluorescence turnover trajectory of a single Au nanoparticle. The digital nature of the stochastic off−on fluorescence bursts and the constant height of the on-level are characteristic of single molecule fluorescence detection. On the basis of control experiments (Supporting Information),[2] we can tell each sudden intensity increase marks the formation of a product Resorufin on the single nanocatalyst. The subsequent intensity decrease marks a dissociation of the product from the nanoparticle surface, and each off−on cycle corresponds to a complete single catalytic turnover according to control experiments (Supporting Information). The actual chemical transformations occur very fast and cannot be resolved in these single molecule fluorescence trajectories. Once the product Resorufin leaves the nanoparticle surface, it becomes undetectable at our imaging rate (100 ms/frame) because of its fast solution-phase diffusion.[2]

In these trajectories, two stochastic waiting times, τ_{off} and τ_{on}, carry the information on reaction kinetics. τ_{off} is the waiting time before each product formation, and τ_{on} is the waiting time for product dissociation after its formation. Resolving τ_{off} and τ_{on} enables examination of the kinetics of catalytic product formation and product dissociation reactions separately. Statistically, $\langle\tau_{off}\rangle^{-1}$ and $\langle\tau_{on}\rangle^{-1}$ ($\langle\ \rangle$ denotes averaging) represent the time-averaged product formation rate and product dissociation rate of single nanocatalyst, respectively. From the classic noncompetitive Langmuir−Hinshelwood mechanism of substrate adsorption on nanocatalysts (Figure 1D),[2] the following single-molecule rate equations connected with conventional kinetic parameters could be obtained

$$\langle\tau_{off}\rangle^{-1} = \gamma_{eff}K_1[S]/(1 + K_1[S]) \quad (1)$$

$$\langle\tau_{on}\rangle^{-1} = (k_2K_2[S] + k_3)/(1 + K_2[S]) \quad (2)$$

where γ_{eff}, the effective rate constant of the product formation process, represents the combined reactivity of all surface sites on one Au nanoparticle, [S] is the concentration of the substrate Resazurin, K_1 is the substrate adsorption equilibrium constant, k_2 is the rate constant of the substrate-assisted product dissociation pathway, k_3 is the rate constant of direct product dissociation, and $K_2 = k_1/(k_{-1} + k_2)$. At saturating Resazurin concentrations, $\langle\tau_{off}\rangle^{-1} \approx \gamma_{eff}$, the effective rate constant for product formation on a single nanocatalyst, and $\langle\tau_{on}\rangle^{-1} \approx k_2$, the rate constant of substrate-assisted product dissociation pathway.

First, we studied the dependence of concentration [S] on the product formation rate ($\langle\tau_{off}\rangle^{-1}$) and dissociation rate ($\langle\tau_{on}\rangle^{-1}$) on single nanocatalysts. Figure S4 shows the Resazurin concentration dependence of $\langle\tau_{off}\rangle^{-1}$ and $\langle\tau_{on}\rangle^{-1}$ on the same set of 18.3 nm individual Au nanoparticles with 5 μM NH_2OH. Each data point is the average over multiple single nanocatalysts. The curves in Figure S4 show that both the average product formation rate ($\langle\tau_{off}\rangle^{-1}$) and dissociation rate ($\langle\tau_{on}\rangle^{-1}$) of a single nanocatalyst saturate when [S] is higher than 30 nM, indicating that $\langle\tau_{off}\rangle^{-1}$ and $\langle\tau_{on}\rangle^{-1}$ could be directly taken as γ_{eff} and k_2, respectively, with [S] > 30 nM for 18.3 nm Au nanoparticles. The saturated product formation rate observed here further confirms that the adsorption of substrate on Au nanoparticles follows the classic noncompetitive Langmuir−Hinshelwood model.[2] On the basis of this observed saturation

DOI: 10.1021/jacs.6b05600
J. Am. Chem. Soc. 2016, 138, 12414−12421

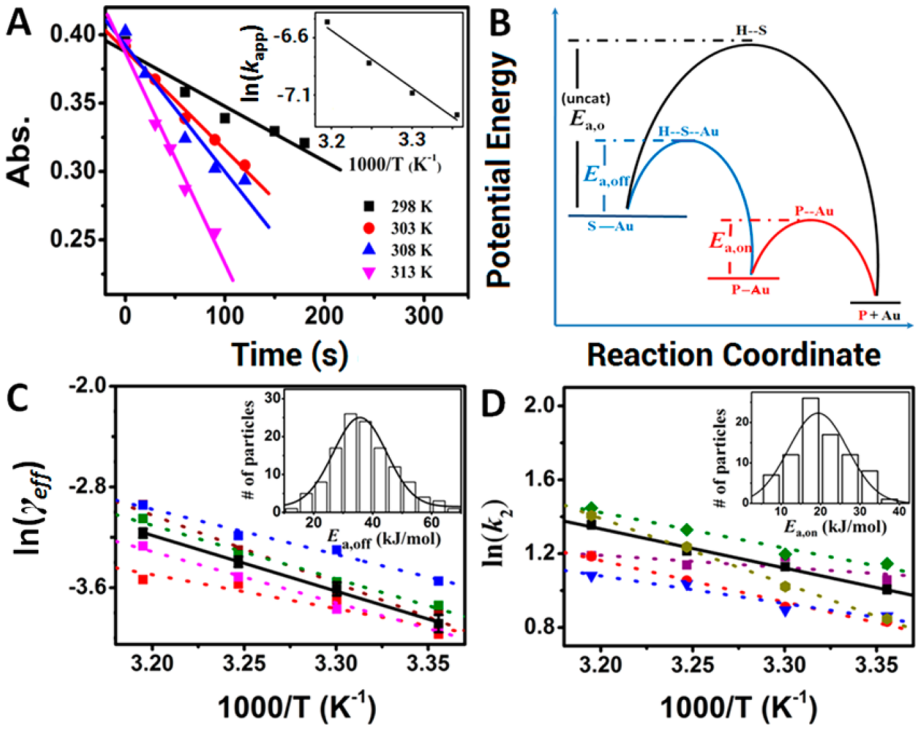

Figure 2. (A) Time-dependent absorption (@600 nm) of Resazurin at different temperatures with 9.1 μM Resazurin, 2 mM NH_2OH, and 0.52 μM Au nanoparticles. Inset: Arrhenius analysis of the apparent rate constants (k_{app}) with temperature gives $E_{a,app}$ = 40.6 ± 3.1 kJ/mol. (B) Schematic energy profile for a reaction proceeding homogeneously (black curve, activation energy uncatalyzed: $E_{a,o}$) and on a surface of Au nanoparticle (blue (for τ_{off} process: $E_{a,off}$) and red (for τ_{on} process: $E_{a,on}$) curves). The term "uncat" was defined as the reaction process without catalyst. (C, D) Arrhenius plot for reactions catalyzed by single Au nanoparticles (dotted lines) and the average over many nanoparticles (full lines) for the product formation process (C) and the product dissociation process (D). Each straight line is the least-squares fit. Inset: the distribution of $E_{a,i}$ from individual nanocatalysts for the product formation process (C) and the product dissociation process (D). Solid lines are Gaussian fits with the center at 35.7 ± 0.5 kJ/mol (inset C) and 19.4 ± 0.6 kJ/mol (inset D).

behavior, subsequent experiments to measure the temperature dependence of the rate constants (γ_{eff} and k_2) were conducted at [S] = 50 nM, as indicated with dotted lines in Figure S4.

Revealing the Activation Energy on Individual Nanocatalysts. Conventional ensemble experiments that vary the reaction temperature can only measure the apparent activation energy ($E_{a,app}$) of the rate-limiting step for an entire (including multiple steps) catalytic process.[14] Similarly, for the case here, the value of $E_{a,app}$ (40.6 ± 3.1 kJ/mol) for the rate-limiting step of the Au-catalyzed fluorogenic reaction shown in Figure 1A was obtained from the ensemble level by analyzing both the temperature- and time-dependent absorption spectrum of the substrate (Figure 2A), although one cannot tell which step is rate-limiting in this multiple-step process (Figure 1D).[3] In contrast, the single-molecule nanocatalysis has the advantage of differentiating a catalytic turnover into a product formation process (τ_{off}) and a product dissociation process (τ_{on}), as shown in Figure 1C.[2] By varying the temperature of single-molecule nanocatalysis, we may derive the activation energy $E_{a,i}$ (i stands for off or on) for these two sequential processes (Figure 2B) on individual nanocatalyst surfaces. From the values of $E_{a,i}$ for these two sequential processes, we can tell which process (product formation process or dissociation process) is rate-limiting.

On the basis of the analysis for the 18.3 nm Au nanoparticles shown in Figure S4, the following Arrhenius equation can be obtained with [S] = 50 nM[16]

$$\langle \tau_{off} \rangle^{-1} = \gamma_{eff} = A_{off} \exp(-E_{a,off}/RT) \quad (3)$$

$$\langle \tau_{on} \rangle^{-1} = k_2 = A_{on} \exp(-E_{a,on}/RT) \quad (4)$$

where A_{off} or A_{on} is the frequency factor of the surface process of τ_{off} or τ_{on}. According to the scheme shown in Figure 1D, $E_{a,off}$ is the activation energy of the product formation process and $E_{a,on}$ is the activation energy of the product dissociation process.

Figure 2C,D reports our observation of the temperature-dependent product formation rate ($\langle \tau_{off} \rangle^{-1}$, or γ_{eff} according to eq 3) and product dissociation rate ($\langle \tau_{on} \rangle^{-1}$, or k_2 according to eq 4) for individual nanocatalysts. From the slopes of Arrhenius equations (eqs 3 and 4) for individual nanocatalysts (Figure 2C,D), we obtained $E_{a,off}$ and $E_{a,on}$ for the two sequential processes on individual nanocatalysts. This is the first measurement of the catalytic activation energy on individual nanocatalysts, especially the simultaneous measurement of $E_{a,off}$ and $E_{a,on}$ for two sequential steps in a catalytic turnover.

The inset in Figure 2C shows the average activation energy ($\langle E_{a,off} \rangle$ = 36.7 ± 1.1 kJ/mol with full width at half-maximum (fwhm) = 21.5 kJ/mol) for the product formation process obtained from multiple Au nanoparticles with widely ranging activation energies of 12–73 kJ/mol (Figure S6). The wide distribution observed here could be mainly attributed to a huge static heterogeneity among Au nanocatalysts (Figures S6 and S7).[2] We can only speculate as to the origin of this heterogeneity in activation energy. It could be due to the tiny differences in either structure (size, shape, or the distribution of active sites on a single nanocatalyst) or the local microenvironment of individual nanocatalysts.[17] Similarly, $\langle E_{a,on} \rangle$ for the product dissociation process on Au nanocatalysts was also

DOI: 10.1021/jacs.6b05600
J. Am. Chem. Soc. 2016, 138, 12414–12421

Table 1. Averaged Activation Energy and Frequency Factors Obtained from Different Methods

	off-reaction			on-reaction		
	method-I	method-II	method-III	method-I	method-II	method-III
$\langle E_{a,i}\rangle$ (kJ/mol)	36.7 ± 1.1	38.2 ± 3.2	33.4 ± 9.2	18.3 ± 1.3	19.3 ± 2.4	21.7 ± 15.4
$\ln(\langle A_i\rangle/s^{-1})$	10.9 ± 0.1	11.4 ± 0.9	10.0 ± 1.9	8.1 ± 0.5	8.6 ± 0.9	8.4 ± 3.3

obtained to be 18.3 ± 1.3 kJ/mol (with fwhm = 17.6 kJ/mol; see inset in Figure 2D). Unsurprisingly, the value of $E_{a,on}$ for individual nanoparticles also varies widely, further confirming catalytic heterogeneity among Au nanocatalysts (Figure S6). The measurement method presented here for $\langle E_{a,i}\rangle$ is referred to as method-I in Table 1. Since $\langle E_{a,off}\rangle$ (36.7 ± 1.1 kJ/mol) is much larger than $\langle E_{a,on}\rangle$ (18.3 ± 1.3 kJ/mol), we conclude that the product formation process is the rate-limiting step. It should be noted here that the $\langle E_{a,off}\rangle$ = 36.7 ± 1.1 kJ/mol obtained from averaging single nanocatalysts is close to the apparent activation energy ($E_{a,app}$ = 40.6 ± 3.1 kJ/mol) obtained from the ensemble experiment. This closeness suggests that the rate-limiting step in this fluorogenic reaction is indeed the product formation process rather than the product dissociation process (Figure 2B). Furthermore, no correlation could be observed between $E_{a,off}$ and $E_{a,on}$ on the same individual nanocatalysts (Figure S8), indicating the product formation process and dissociation process are independent of each other. This may be because the active sites for product formation are different from the docking sites on which the product molecules dissociate,[2] since product diffusion on the surface of individual nanocatalysts has been observed in single-molecule imaging.[12] Moreover, the spontaneous or catalysis-induced reconstruction of active sites is another possible reason for the observation of no correlation (Figure S8) or different activation energies obtained for product formation and dissociation processes, since the reconstruction of active sites can affect the catalytic process.[2]

Compensation Effect of Individual Nanocatalysts and the Isokinetic Relationship. For the compensation effect in heterogeneous catalysis, it was found that, when the catalytic activation energy (E_a) changes, so does the frequency factor (A).[25] Simply, these two parameters correlate with each other as follows

$$\ln A \propto \beta \cdot E_a \tag{5}$$

where β, the proportionality constant, could be positive or negative.[22] In order to confirm whether the compensation effect is also applicable to single nanocatalysts or not, we studied the correlation of the obtained $E_{a,i}$ and A for multiple individual nanocatalysts. Interestingly, as shown in the Constable plot (Figure 3A,B), almost all data point pairs ($E_{a,i}$, $\ln(A_i)$) are perfectly linearly correlated, indicating an apparent compensation effect. Surprisingly, the obtained proportionality constants (β) (the slopes shown in Figure 3A,B) between $E_{a,off}$ and A_{off} and between $E_{a,on}$ and A_{on} were found to be exactly the same with a value of 0.39 mol/kJ, while the isokinetic temperature (T_{iso}), a fundamentally important temperature at which all reactions of the series should proceed at the same rate, was estimated to be about 308 K (35 °C) from the relationship of $\beta = 1/(RT_{iso})$.[21,22]

However, does the linear relationship observed here really reflect the compensation effect? Or, are the values of T_{iso} obtained from the slopes really reliable? According to a previous report,[22] as shown in the Supporting Information, when the temperature varies in a narrow range (such as for a temperature range $[T_2 \sim T_1]$, $T_1 > T_2$, and $T_2/T_1 \approx 1$ with temperature in K), the following relationship about the slope (β) of the linear dependence of $\ln(A)$ on E_a could be obtained (Supporting Information)

$$1/(RT_1) \le \beta = 1/(RT_{iso}) \le 1/(RT_2) \tag{6}$$

which results in the relationship $T_2 \le T_{iso} \le T_1$.[23,24] This relationship explains why the same slopes were obtained (Figure 3A,B) or why the T_{iso} value obtained here is within the temperature range 298−313 K for both the product formation process and the dissociation process. Equation 6 further states that the value of T_{iso} only depends on and shifts with the temperature window of $[T_2 \sim T_1]$ if $T_2/T_1 \approx 1$ and has nothing to do with the intrinsic (catalytic) properties of reaction systems. However, this prediction is obviously false, since T_{iso} represents a special temperature at which all reactions in the

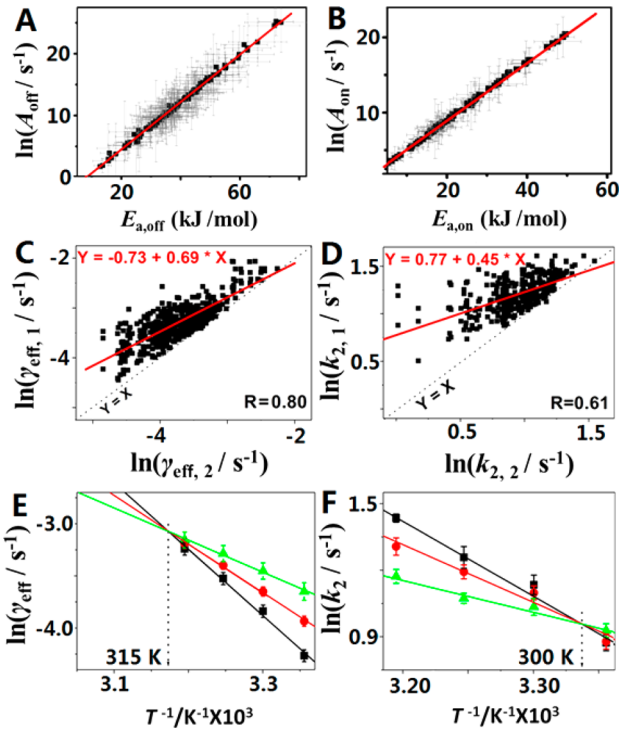

Figure 3. Isokinetic relationship or compensation effect in the single-molecule catalysis of individual Au nanoparticles. (A, B) Constable plot of the frequency factors versus the activation energies, obtained from many individual nanoparticles that catalyze the product formation process (A) and the dissociation process (B). Red lines are linear fits with R = 0.99 (A) and R = 0.99 (B). (C, D) Dependence of kinetic rate constants ((C) for $\ln \gamma_{eff}$, (D) for $\ln k_2$) on individual nanocatalysts at two temperatures (T_1, T_2, $T_1 > T_2$, in this case, T_1: {303 K, 308 K; 313 K}; T_2: {298 K, 303 K; 308 K}). (E) Isokinetic relationship of three groups of individual nanoparticles with different average $E_{a,off}$ in the coordinates T^{-1} and $\ln \gamma_{eff}$. The solid lines are the linear fittings. (F) Isokinetic relationship of three groups of individual nanoparticles with different average $E_{a,on}$ in the coordinates T^{-1} and $\ln k_2$. The solid lines are the linear fittings.

DOI: 10.1021/jacs.6b05600
J. Am. Chem. Soc. 2016, 138, 12414−12421

series proceed at the same rate and should be a characteristic constant for a particular reaction system.[22] This fact means that the T_{iso} cannot be obtained reliably from a Constable plot especially when the temperature window adopted is very narrow. Even though the apparent compensation effect has a mathematical origin, it is not accurate to invoke any physicochemical explanation, since the observed effect probably has little predictive power.[23,24]

Indeed, Exner had reported, when $T_1/T_2 \approx 1$, the apparent correlations between the activation parameters sometimes (such as the Constable plot shown in Figure 3A,B) do not necessarily originate from the correlated rate constants at different temperatures.[22] He further suggested that the actual relationships between the activation parameters can be reliably checked by plotting $\ln k_{i,1}$ vs $\ln k_{i,2}$ (Supporting Information). In this case, the rate constant k_i represents either γ_{eff} for the product formation process or k_2 for the product dissociation process on individual nanoparticles. $k_{i,1}$ and $k_{i,2}$ are the values of the rate constant k_i at two random temperatures T_1 and T_2, respectively ($T_1 > T_2$). Interestingly, as shown in Figure 3C,D, both γ_{eff} and k_2 show positive correlations (correlation coefficients R = 0.80 and 0.61 for γ_{eff} and k_2, respectively), indicating that the activation parameters indeed compensate one another (compensation law).[22] The positive slopes (Figure 3C,D and Figure S9) less than unity for both γ_{eff} and k_2 indicate that the selectivity of the catalytic reaction diminishes with increasing temperature.[22] The differences in correlation coefficients and slopes between γ_{eff} and k_2 indicate different compensation behaviors between the product formation process and dissociation process, consistent with the observation of no correlation between $E_{a,off}$ and $E_{a,on}$ (Figure S8). The larger values of correlation coefficient and slope for γ_{eff} than those for k_2 probably indicate that the activation parameters for the product formation process correlate with one another more tightly than the product dissociation process.

In order to further determine the value of the isokinetic temperature (T_{iso}) for both product formation and dissociation processes, we divided the individual nanoparticles studied here (insets shown in Figure 2C,D) into three subgroups according to the values of the activation energies for both the product formation process (small with $E_{a,off} \leq 30$ kJ/mol, middle with $30 < E_{a,off} \leq 42$ kJ/mol, and large with $E_{a,off} > 42$ kJ/mol) and the dissociation process (small with $E_{a,on} \leq 15$ kJ/mol, middle with $15 < E_{a,on} \leq 25$ kJ/mol, and large with $E_{a,on} > 25$ kJ/mol). From each group, an average isokinetic relationship in the coordinates T^{-1} and $\ln k_i$ was obtained corresponding to an individual $\langle E_{a,i} \rangle$. It should be noted here that these three groups of individual nanoparticles are equivalent to three sets of nanocatalysts with different barriers in the activation process.[21] Interestingly, as shown in Figure 3E,F, the three independent average lines for both the product formation process and the dissociation process intersect in one point, respectively, the abscissa of which gives the isokinetic temperature T_{iso} of 315 K for the product formation process and 300 K for the product dissociation process. Interestingly, the value of T_{iso} (315 K) for the product formation process is out of the temperature range of 298−313 K, while the value of T_{iso} (300 K) for the product dissociation process is within the range. The lower T_{iso} for the product dissociation process than that for the product formation process probably indicates a lower energy barrier for the product dissociation process, consistent with the average $E_{a,i}$ shown in Table 1.

Many attempts have been made to explain the origin of the compensation effect for heterogeneous catalysis.[18,26] It has been found that the compensation effect appears in catalysis when the effect on activation energy (E_a) caused by changes in surface coverage is balanced out by the entropic configuration contributions of the surface.[21] According to a switching theory,[18] the compensation effect in catalysis could be attributed to the kinetic switching for coupled surface reactions and is intimately linked to an underlying linear relationship between the activation energy (E_a) and the stability of surface species, which has been known to be able to modulate the coverage of free sites and in turn affects both E_a and the frequency factor A.[21] As for the importance or roles of the compensation effect in chemical reactions, it has been known that the compensation effect could be useful in chemical research for identifying the governing reaction mechanism, predicting Arrhenius parameters when limited data are available, predicting effects of various parameters on reactions, separating the effects of surface and bulk properties, and optimizing process design.[27] For example, Ranganathan et al. successfully demonstrated how the compensation effect can be effectively used to separate the effects of surface and bulk properties.[28] It should be noted this is the first observation of the compensation effect at the single-particle level as well as the first measurement of T_{iso} for both a product formation process and a dissociation process within one catalytic cycle. The work presented here deepens our understanding or cognition to the catalysis and provides a new single-molecule single-particle method for the measurement of the fundamentally important parameter T_{iso},[22] which is potentially useful for the optimization of process design.[27]

Activity Distribution and Correlation to Activation Energy. Furthermore, Figure 4A and B show the broad distributions of both γ_{eff} and k_2 for many individual Au nanocatalysts at four different temperatures. From Gaussian fittings of these distributions, we obtained the temperature-dependent average rate constants ($\langle \gamma_{eff} \rangle$ and $\langle k_2 \rangle$). Similarly, on the basis of the Arrhenius equations (eqs 3 and 4) (insets in

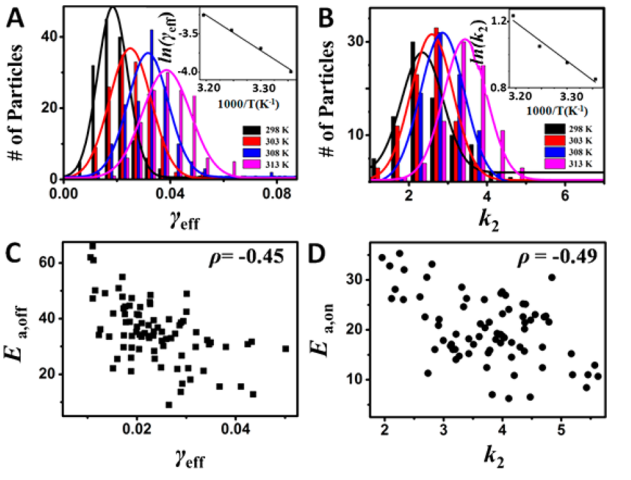

Figure 4. (A, B) Distributions of γ_{eff} (A) and k_2 (B) of different temperatures from individual Au nanoparticles. Solid lines are Gaussian fits. Insets: Arrhenius analysis of the centers of Gaussian fits from parts A and B. (C, D) Correlation analysis between the catalytic activity (γ_{eff} (C) and k_2 (D)) and activation energy of individual Au nanoparticles at 25 °C. Each data point is from one Au nanoparticle.

DOI: 10.1021/jacs.6b05600
J. Am. Chem. Soc. 2016, 138, 12414−12421

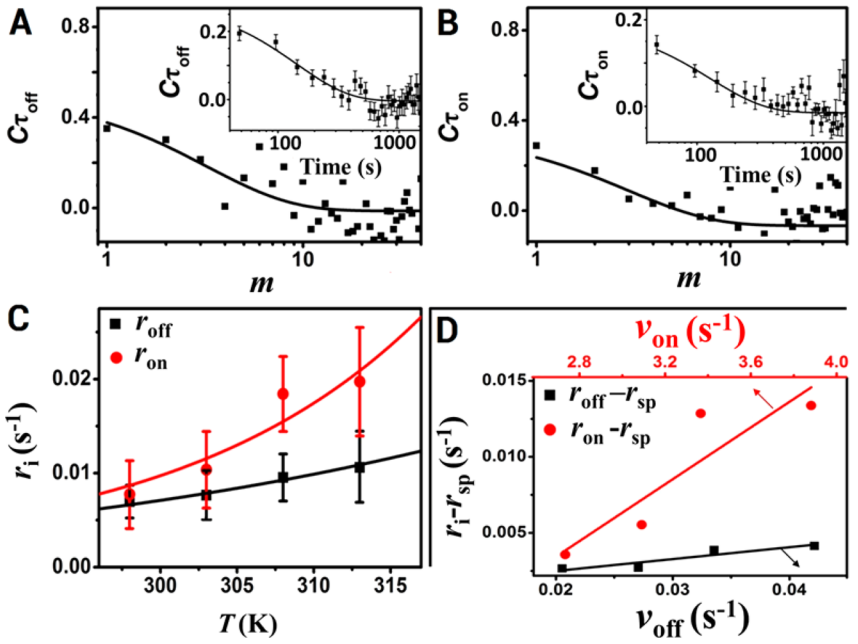

Figure 5. (A, B) Autocorrelation functions of τ_{off} (A) and τ_{on} (B) from the turnover trajectory of a single Au nanocatalyst. Solid lines are exponential fits with decay constants of $m_{off} = 3.8 \pm 1.1$ turnovers and $m_{on} = 2.7 \pm 0.9$ turnovers. Insets: Autocorrelation functions of the reaction time t from the turnover trajectories of Au nanoparticles. The x-axis was converted from the turnover index m to real time using the average turnover time of each nanoparticle. Solid lines are exponential fits. (C) Temperature dependence of the activity fluctuation rate of Au nanoparticles in catalysis. Solid lines are fittings with eqs 9 (black line) and 10 (red line). (D) Temperature dependence of the catalysis-induced surface restructuring rate of Au nanocatalysts. Red symbols: the τ_{on}-induced surface restructuring rate ($p_{on}\nu_{on} = r_{on} - r_{sp}$). Black symbols: the τ_{off}-induced surface restructuring rate ($p_{off}\nu_{off} = r_{off} - r_{sp}$); solid lines are linear fittings.

Figure 4A,B), we obtained the frequency factors $\ln(A_{off}/s^{-1}) = 11.4 \pm 0.9$ and $\ln(A_{on}/s^{-1}) = 8.6 \pm 0.9$ and the average activation energy $\langle E_{a,off}\rangle = 38.2 \pm 3.2$ kJ/mol and $\langle E_{a,on}\rangle = 19.3 \pm 2.4$ kJ/mol for the product formation and dissociation process, respectively. Interestingly, these values are very close to those obtained from the averaging of multiple individual $E_{a,i}$, as shown in Figure 2 or Table 1 (method-I).The measurement method presented here for $\langle E_{a,i}\rangle$ was named method-II. The consistency of these two sets of data indicates the reliability of the experiments and analytic method presented here.

To further evaluate the correlation between catalytic activity and activation energy at the single nanocatalyst level, we plotted $E_{a,off}$ versus γ_{eff} and $E_{a,on}$ versus k_2, respectively, for multiple individual nanocatalysts. Interestingly, parts C and D of Figure 4 show that the Pearson cross correlation coefficients (ρ) are -0.45 ± 0.04 (the error bar here is the probable error of the correlation coefficient)[29] for the product formation process and -0.49 ± 0.06 for the product dissociation process. This indicates a smaller activation energy corresponds to a higher intrinsic catalytic activity for both the product formation process and the product dissociation process. It also confirms prior reports that a reaction is easier if the activation energy is smaller.[30] This fact further indicates that the compensation effect of the frequency factor (A) to E_a is incomplete, or that the k-increase induced by the increase of A could ***only*** compensate part of the k-decrease induced by the increase of E_a due to the faster decreasing rate of the exponential function with E_a increase ($\propto \exp(-E_a/RT)$) than the linear increasing rate of linear function with A increase ($\propto A$).

Thermal-Induced Dynamic Fluctuation of Catalytic Activity. Nanocatalysts are usually unstable and can restructure dynamically, especially under turnover conditions, where the constantly fluctuating adsorbate−surface interactions can further induce dynamic surface restructuring.[31] Furthermore, the surface restructuring can cause temporal variations on catalytic activity of individual nanoparticles. The temporal dynamics of catalytic activity has been observed in single-molecule experiments on Au nanoparticles. These time-varying fluctuations in catalytic activity are likely attributable to spontaneous and catalysis-induced dynamic surface restructuring.[2] The time scale of the activity fluctuations, which is also the time scale of the underlying surface restructuring, can be obtained from the autocorrelation function $C_\tau(m) = \langle \Delta\tau(0)\Delta\tau(m)\rangle/\langle \Delta\tau^2\rangle$. Here, τ is either τ_{off} or τ_{on}, m is the turnover index number in the sequence, and $\Delta\tau(m) = \tau(m) - \langle\tau\rangle$. In the presence of activity fluctuations, $C_\tau(m) \geq 0$ and shows a decay behavior with the decay time constant being the fluctuation correlation time.[32]

Parts A and B of Figure 5 show exemplary $C_{\tau_{off}}(m)$ and $C_{\tau_{on}}(m)$ of a single Au nanocatalyst with a size of about 18.3 nm. The exponential decay behaviors of $C_{\tau_{off}}(m)$ and $C_{\tau_{on}}(m)$ directly demonstrate the fluctuations of catalytic activity for the product formation and product dissociation processes at 25 °C, respectively. For the single nanocatalyst shown in Figure 5A,B, the exponential decay constant of $C_{\tau_{off}}(m)$ is $m_{off} = 3.8 \pm 1.1$ turnovers, and that of $C_{\tau_{on}}(m)$ is $m_{on} = 2.7 \pm 0.9$ turnovers. $C_{\tau_{off}}(m)$ and $C_{\tau_{on}}(m)$ of each nanocatalyst can then be converted to $C_{\tau_{off}}(t)$ and $C_{\tau_{on}}(t)$ in which the turnover index m is converted to real time t using the average turnover time of the single nanoparticle.[29] When $C_{\tau_{off}}(t)$ and $C_{\tau_{on}}(t)$ are averaged over many nanoparticles, their exponential decay behavior is preserved (Figure 5A,B inset). The two corresponding decay time constants are $t_{off} = 143.3 \pm 25.5$ s and $t_{on} = 129.8 \pm 31.2$ s, which are the activity fluctuation time scales for the product

DOI: 10.1021/jacs.6b05600
J. Am. Chem. Soc. 2016, 138, 12414−12421

formation and dissociation processes, respectively, and also reflect the corresponding time scales of the underlying dynamic surface restructuring of the Au nanoparticle. The inverse of these two time scales corresponds to the surface restructuring rates (r_i, i = off or on) of single nanocatalysts during the τ_{off} process and the τ_{on} process, respectively.

We further studied the temperature dependence of r_i at fixed substrate concentration ([S] = 50 nM). As shown in Figure 5C, the positive correlation between r_i and temperature indicates that the dynamic activity fluctuation or surface restructuring is indeed thermal-induced due to the temperature-dependent spontaneous dynamic surface restructuring (r_{sp}, the spontaneous surface restructuring rate) and catalysis-induced surface restructuring ($p_i v_i$, the catalysis-induced surface restructuring rate, p_i is a proportionality constant that couples the catalysis process (off or on process) to surface restructuring, v_i is the product formation rate (v_{off}) or dissociation rate (v_{on})), and[3]

$$r_i = r_{sp} + p_i v_i \tag{7}$$

$$r_{sp} = r_{sp}^0 \exp(-\Delta E_{sp}/RT) \tag{8}$$

$$v_{off} = \langle \tau_{off} \rangle^{-1} = \gamma_{eff} = A_{off} \exp(-E_{a,off}/RT) \tag{3a}$$

$$v_{on} = \langle \tau_{on} \rangle^{-1} = k_2 = A_{on} \exp(-E_{a,on}/RT) \tag{4a}$$

Combining the above equations, the temperature-dependent surface restructuring rates (r_i) of τ_{off} and τ_{on} processes could be obtained as follows

$$r_{off} = r_{sp}^0 \exp(-\Delta E_{sp}/RT) + q_{off} \exp(-E_{a,off}/RT) \tag{9}$$

$$r_{on} = r_{sp}^0 \exp(-\Delta E_{sp}/RT) + q_{on} \exp(-E_{a,on}/RT) \tag{10}$$

where $q_i = p_i A_i$. By fitting the temperature dependence of r_i based on eqs 9 and 10 with $r_{sp}^0 = 20 \pm 18$ s^{-1} and $\Delta E_{sp} = 20.9 \pm 3.2$ kJ/mol adopted from ref 3, as shown in Figure 5C, we obtain $q_{off} = 1650 \pm 320$ s^{-1}, $\langle E_{a,off} \rangle = 33.4 \pm 9.2$ kJ/mol and $q_{on} = 38 \pm 15$ s^{-1}, $\langle E_{a,on} \rangle = 21.7 \pm 15.4$ kJ/mol. The measurement method presented here for $\langle E_{a,i} \rangle$ was named method-III. These values are consistent with those obtained above from method-I and method-II (Table 1).

On the other hand, on the basis of the values of r_{sp} at different temperatures obtained from eq 8 with $r_{sp}^0 = 20 \pm 18$ s^{-1} and $\Delta E_{sp} = 20.9 \pm 3.2$ kJ/mol adopted from ref 3, from eqs 3a and 4a and eqs 9 and 10, we can get the pure catalysis-induced surface restructuring rate, $p_i v_i$, which is equal to $r_i - r_{sp}$ according to eq 7. As shown in Figure 5D, the linear fittings between $p_i v_i$ and v_i give the proportionality constants (p_i) for two processes, $p_{off} = 0.078 \pm 0.021$ and $p_{on} = 0.009 \pm 0.003$. On the basis of the obtained $q_{off} = 1650 \pm 320$ s^{-1} and $q_{on} = 38 \pm 15$ s^{-1}, we derived the frequency factors from the relationship of $q_i = p_i A_i$: $\ln(A_{off}) = 10.0 \pm 1.9$ and $\ln(A_{on}) = 8.4 \pm 3.3$. Interestingly, as shown in Table 1, these two values are also consistent with those previously obtained from method-I and method-II. The consistency across these three data analysis methods provides us greater confidence in the reliability of the experiments and analytic method presented here.

CONCLUSION

By monitoring the temperature-dependent catalytic activity of single Au nanocatalysts, we have successfully derived the activation energies using three different methods for two sequential catalytic steps on single nanocatalysts. A large static heterogeneity among the individual nanocatalysts was observed. The compensation effect and the isokinetic relationship of catalytic reactions were observed at the single particle level. This study helps to deepen the understanding of heterogeneous nanocatalysis at the single-particle level.

EXPERIMENTAL METHODS

Temperature-Controllable Single-Molecule Experiments. On the basis of a temperature controllable flow cell, single-molecule fluorescence measurements were performed on a home-built TIRF microscope. A continuous wave circularly polarized 532 nm laser beam was focused to directly excite the fluorescence of Resorufin. The fluorescence of Resorufin was collected and projected onto an EMCCD camera. A series of movies was collected at different temperatures. The movies are analyzed using a home-written IDL program from localized fluorescence spots individually across the entire movie (Supporting Information).

ASSOCIATED CONTENT

Supporting Information

The Supporting Information is available free of charge on the ACS Publications website at DOI: 10.1021/jacs.6b05600.

Detailed experimental methods; UV/vis spectral of ensemble measurement, image of experimental setup, histogram of size distribution, control experiment, error analysis, correlation analysis and slope of constable plot in supplementary Figures S1−S9 (PDF)

AUTHOR INFORMATION

Corresponding Author

*weilinxu@ciac.ac.cn

Notes

The authors declare no competing financial interest.

ACKNOWLEDGMENTS

We thank Prof. Gabor A. Somorjai from UC Berkeley, Prof. Gerhard Ertl from Fritz-Haber-Institut der Max-Planck-Gesellschaft in Berlin, Germany, and Prof. Kaitlin Bratlie from Iowa State University for their suggestions and comments on the analysis of the compensation effect and isokinetic relationship during the manuscript revision process. Work was funded by the National Basic Research Program of China (973 Program, 2014CB932700, and 2012CB932800), National Natural Science Foundation of China (21422307, 21303180, 21433003, 21573215, 21503212, and 21503211), "the Recruitment Program of Global youth Experts" of China, Science and Technology Innovation Foundation of Jilin Province for Talents Cultivation (20160519005JH), and Jilin Youth foundation (20160520137JH).

REFERENCES

(1) Somorjai, G. A.; Li, Y. *Introduction to surface chemistry and catalysis*; Wiley-Interscience: New York, 2010.

(2) Xu, W.; Kong, J. S.; Yeh, Y.-T. E.; Chen, P. *Nat. Mater.* **2008**, *7*, 992.

(3) Zhou, X.; Xu, W.; Liu, G.; Panda, D.; Chen, P. *J. Am. Chem. Soc.* **2010**, *132*, 138.

(4) Andoy, N. M.; Zhou, X.; Choudhary, E.; Shen, H.; Liu, G.; Chen, P. *J. Am. Chem. Soc.* **2013**, *135*, 1845.

(5) Novo, C.; Funston, A. M.; Mulvaney, P. *Nat. Nanotechnol.* **2008**, *3*, 598.

(6) Tachikawa, T.; Majima, T. *J. Am. Chem. Soc.* **2009**, *131*, 8485.

(7) Tachikawa, T.; Yamashita, S.; Majima, T. *Angew. Chem.* **2010**, *122*, 442.

DOI: 10.1021/jacs.6b05600
J. Am. Chem. Soc. 2016, 138, 12414−12421

(8) Tachikawa, T.; Yamashita, S.; Majima, T. *J. Am. Chem. Soc.* **2011**, *133*, 7197.
(9) Wang, N.; Tachikawa, T.; Majima, T. *Chem. Sci.* **2011**, *2*, 891.
(10) Tachikawa, T.; Yonezawa, T.; Majima, T. *ACS Nano* **2013**, *7*, 263.
(11) Ha, J. W.; Ruberu, T. P. A.; Han, R.; Dong, B.; Vela, J.; Fang, N. *J. Am. Chem. Soc.* **2014**, *136*, 1398.
(12) Roeffaers, M. B.; Sels, B. F.; Uji-i, H.; De Schryver, F. C.; Jacobss, P. A.; De Vos, D. E.; Hofkens, J. *Nature* **2006**, *439*, 572.
(13) Roeffaers, M. B. J.; Cremer, G. D.; Libeert, J.; Ameloot, R.; Dedecker, P.; Bons, A. J.; Buckins, M.; Martens, J. A.; Sels, B. F.; Vos, D. E. D.; Hofkens, J. *Angew. Chem., Int. Ed.* **2009**, *48*, 9285.
(14) Grunes, J.; Zhu, J.; Anderson, E. A.; Somorjai, G. A. *J. Phys. Chem. B* **2002**, *106*, 11463.
(15) Moseler, M.; Walter, M.; Yoon, B.; Landman, U.; Habibpour, V.; Harding, C.; Kunz, S.; Heiz, U. *J. Am. Chem. Soc.* **2012**, *134*, 7690.
(16) Satterfield, C. N. *Heterogeneous catalysis in practice*; McGraw-Hill: New York, 1980.
(17) Craig, D. B.; Arriaga, E. A.; Wong, J. C. Y.; Lu, H.; Dovichi, N. J. *J. Am. Chem. Soc.* **1996**, *118*, 5245.
(18) Bligaard, T.; Honkala, K.; Logadottir, A.; Nørskov, J. K.; Dahl, S.; Jacobsen, C. J. H. *J. Phys. Chem. B* **2003**, *107*, 9325.
(19) Wilson, H. A. *Philos. Trans. R. Soc., A* **1908**, *208*, 247.
(20) Wilson, M. C.; Galwey, A. K. *Nature* **1973**, *243*, 402.
(21) Teschner, D.; Novell-Leruth, G.; Farra, R.; Knop-Gericke, A.; Schlögl, R.; Szentmiklósi, L.; Hevia, M. G.; Soerijanto, H.; Schomäcker, R.; Pérez-Ramírez, J.; López, N. *Nat. Chem.* **2012**, *4*, 739.
(22) Exner, O. *Nature* **1964**, *201*, 488.
(23) Barrie, P. J. *Phys. Chem. Chem. Phys.* **2012**, *14*, 327.
(24) Barrie, P. J. *Phys. Chem. Chem. Phys.* **2012**, *14*, 318.
(25) Palmer, W. G.; Constable, F. H. *Proc. R. Soc. London, Ser. A* **1924**, *106*, 251.
(26) Constable, F. H. *Proc. R. Soc. London, Ser. A* **1925**, *108*, 355.
(27) Agrawal, R. K. *J. Therm. Anal.* **1988**, *34*, 1141.
(28) Ranganathan, R.; Bakhshi, N. N.; Mathews, J. F. *Can. J. Chem. Eng.* **1977**, *55*, 544.
(29) Han, K. S.; Liu, G.; Zhou, X.; Medina, R. E.; Chen, P. *Nano Lett.* **2012**, *12*, 1253.
(30) Somorjai, G. A.; Contreras, A. M.; Montano, M.; Rioux, R. M. *Proc. Natl. Acad. Sci. U. S. A.* **2006**, *103*, 10577.
(31) Imbihl, R.; Ertl, G. *Chem. Rev.* **1995**, *95*, 697.
(32) Lu, H. P.; Xie, X. S. *Nature* **1997**, *385*, 143.

DOI: 10.1021/jacs.6b05600
J. Am. Chem. Soc. 2016, 138, 12414−12421